Exergy And Performance Analysis of A CO2 Single Stage Thermal Compressor Heat Pump

Ali Salame[1,2,3], Vincent Lemort[2], Pascal Dufour[3], Madiha Nadri[3]

[1] Boostheat Company, Lyon, France
[2] University of Liège, Energy Systems Research Unit, Liège, Belgium
[3] Univ Lyon, Université Claude Bernard Lyon 1, CNRS, LAGEPP UMR 5007, 43 boulevard du 11 novembre 1918, F-69100, VILLEURBANNE, France,
ali.salame@boostheat.com

Abstract. A thermal compressor heat pump is a thermally driven heat pump application that mainly uses thermal energy to drive a compression cycle, delivering heat to the user. The thermal energy can be in the form of waste heat, combustion of natural gas, or solar, which would contribute to the demand for higher-efficiency machines and decreasing greenhouse gas emissions. The thermal energy is directly received by the thermal compressor, which aims to convert it into compression power, replacing a conventional electric compressor. Exergy analysis is gaining more interest today as it offers a deep and detailed analysis of the inefficiencies in a system. Such analysis highlights the highest deficiencies in components and the maximum possible potential for process optimization. Being an important component, an overall performance optimization of a thermal compressor heat pump cannot bypass the optimization of its compressor. For this reason, we carry out an exergy analysis on the thermal compressor integrated into a single-stage heat pump cycle, based on previously derived data-driven models. A parametric exergy analysis is carried out to find the optimal operating conditions at the level of a thermal compressor first, and second on a single-stage thermal compressor heat pump cycle.

Keywords: Thermal Compressor, Exergy Analysis, CO2, Heat pump

1 Introduction

Due to the increase in energy demand followed by an increase in global warming and ozone layer depletion, heat pumps are gaining more attention than ever. The use of a natural refrigerant like CO2 makes heat pumps more environmentally friendly, although more complex, due to the physical characteristics of CO2 characterized by a high critical pressure of 73.8 bar and a low critical temperature of 31.3 °C [1]. 99% of heat pump applications use electricity as the primary energy source and only 1% uses a heat energy source, which does not receive much attention today [2].

One application is a thermal compressor heat pump (TCHP) developed by Boostheat, which uses a three-stage thermal compressor (TC) cycle to reach the high-critical pressure of CO2 where performance is at its highest. The TC is a Stirling-type machine with inlet and outlet valves instead of a power piston [3]. The pressure inside is increased by increasing the temperature rather than density induced by mechanical power. This being said, conventional metrics such as isentropic and volumetric efficiencies are avoided, and direct empirical correlations for mass flow rate and discharge temperature are considered [4].

Analyzing the performance of a TCHP is an important key to understanding the efficiency and energy utilization under varying operational conditions and can help in system optimization. To quantify the performance of a heat pump cycle, an energy analysis based on the first law has always been widely used. The sufficiency of this metric has been questioned by several authors, proposing a second law efficiency as a more concrete evaluation metric for heat pump performance [5].

For a heat pump cycle, the thermodynamic inefficiencies in components were identified, and the importance of using exergetic analysis instead of the coefficient of performance (COP) was highlighted [6]. Exergy analysis, inspired by the second law, is getting more attention today, as it provides a qualitative analysis that identifies the potential (maximum) useful energy that can be recovered from a system [7]. As a deeper analysis, it points out how, where, and the amount of performance degraded in a cycle, thus providing clues about potential improvements. Several works have been done to highlight the importance of exergy-based analysis on vapor compression cycles.

Badescu [8] conducted an exergy analysis on a solar-assisted heat pump for heating, concluding that exergy losses are mainly due to compression and condensation. Yang et al. [9] carried out an exergy analysis on a transcritical CO2 refrigeration cycle with an expander, showing that replacing a throttle valve with an expander would reduce the total exergy lost due to the expansion process by 50%. Also, for refrigeration compression cycles, a comparative and exergy analysis was carried out with different refrigerants and cycle configurations, concluding that CO2 cycles can achieve good exergy efficiency when operating at optimal temperatures with advanced configurations like two-stage compression and effective internal heat exchangers [10]. An exergy analysis review for vapor compression refrigeration cycles concluded that the largest exergy loss more frequently occurred in a compressor and that the temperature difference between evaporation and condensation should be kept as small as possible [11]. A system undergoes a reversible process if both the system and the surroundings can be restored to their initial states without leaving any net change, which is impossible in reality. The irreversibilities found in a heat pump cycle include friction and heat transfer losses. Most of literature work is on CO2 transcritical cycle, where higher sink temperatures can be achieved. Since our ss-TCHP is only subcritical cycle due to the data range of a TC and its low-pressure ratio, a comparison is not fair here.

A Stirling-type TC with inlet and outlet valves is used instead of a conventional compressor. An exergy analysis of this unique component is also needed. For a Stirling-type TC—a critical component of Vuilleumier machines—Wang et al. [12] have investigated the internal heat-work conversion and loss processes which suffer from low efficiency due to various losses. By developing a reliable third-order model, analyzing parameter effects, and proposing optimization strategies, the study aimed to enhance the exergy efficiency of a Stirling-type TC to 60%. To develop and demonstrate an exergy-based method for analyzing a reciprocating compressor's performance, the inefficiencies caused by friction, irreversible heat transfer, throttling, and fluid mixing are quantified and identified with correlations [13]. On the other hand, this work aims to give empirical (data-based) correlations for the five main performance predictions as a function of the four main inputs, when a TC is integrated into a single-stage TCHP (ss-TCHP). The goal is to identify the optimal operating conditions of a TC based on an exergy analysis. The exergy analysis is extended to cover other cycle components such as the condenser, evaporator, and expansion valve, where exergy destruction at each is calculated and then compared.

2 Single Stage Thermal Compressor Heat Pump

2.1 Thermal Compressor Processes

Unlike a traditional compressor, a thermal compressor does not rely on volume variation to create pressure waves, but rather on thermal energy. One way to describe the thermodynamic process is to show the uniform pressure variation inside the compressor as a function of the displacer movement X_D. The four processes are represented in Fig. 1. From phase 1 to 2, the downward movement of the displacer transports the CO2 to the upper hot part of the cylinder. Due to the high temperature, the fluid pressure gradually increases. When the pressure is high enough, the exhaust valve opens, and CO2 maintains a constant pressure from 2 to 3, assuming no pressure drop associated with the flow through the valves. At phase 3 the displacer reverses its direction of movement, and the CO2 moves again to the lower cold part, causing the gradual decrease of pressure. When the pressure is low enough (at phase 4), inlet valve opens, and CO2 returns to its initial state at 1.

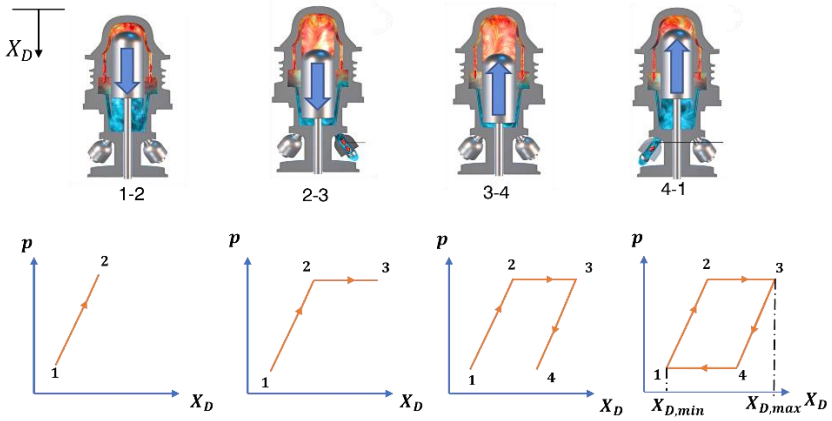

Fig. 1: The variation of pressure $\boldsymbol{p}$ as a function of displacement $\boldsymbol{X_D}$.

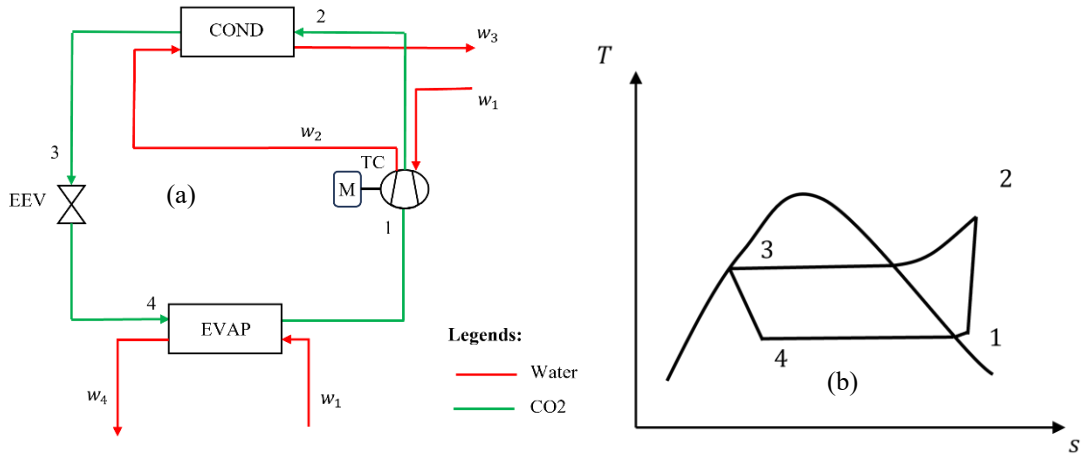

Fig. 2: (a) Test Bench layout with (b) the T-s diagram of CO2 in a ss-TCHP cycle**.**

2.2 Test Bench Layout

To investigate the performance of a TC, it was installed in a basic heat pump cycle as shown in Fig. 2(a), which we refer to as a ss-TCHP. This setup includes a TC, a condenser (COND), an electronic expansion valve (EEV), and an evaporator (EVAP). The EEV is manually adjusted to regulate the pressure ratio, so that a minimum valve opening corresponds to maximum pressure ratio and vice versa. The CO2 in the cycle remains in its subcritical state, as depicted in the T-s diagram in Fig. 2(b). The TC receives heat from its top part by a combustion process, where the heat absorbed is ($\dot{Q}_{heater}$). An electric motor (M) with power ($\dot{W}_m$) is connected to the displacer to ensure its movement, although it operates with relatively low power compared to the heating power. Part of the resulting power is recovered by the cooling water ($\dot{Q}_{cooler}$) that circulates around the cooler in a water jacket, another is lost to the ambient as ($\dot{Q}_{loss}$), and the remainder is released to the thermal cycle as output enthalpy flow (T_2 and $\dot{m}$). The compression phase of the CO2 is represented by 1-2, which proceeds through a desuperheating and condensation process in 2-3. After expansion occurs in the EEV from 3 to 4, evaporation and superheating occur, transitioning the state of CO2 back to 1. Details about collected data can be found in [4].

2.3 Data-Driven Models for A TC

A crucial aspect of understanding a TC lies in examining the energy conversion processes and the thermal losses within the system. The primary energy input comes from heat energy, generated by an external combustion process at the top of the heater. Additionally, electrical energy powers the motor, which converts it into mechanical energy transmitted by the displacer to the CO2 inside the compressor. In some cases, this additional energy input may not be necessary and can even be recovered. The useful energy output comprises the increase in the enthalpy flow of the CO2 (reflecting the pressure rise) and the heat recoverable from the low-temperature source, as illustrated in Fig. 3(a). The models are exclusive for a certain TC design. Based on collected data of 256 samples from a ss-TCHP (Fig. 2(a)), data-driven models were derived to predict the main performance indicators of a TC. ($\dot{Q}_{heater}, \dot{Q}_{cooler}, \dot{m}, T_{out}, \dot{W}_m$, and $\dot{Q}_{loss}$) based on inputs: inlet pressure p_1, outlet pressure p_2, heater temperature T_{heater}, water temperature T_{w1}, motor speed ω, and inlet temperature T_1 [4]. The neural network models have shown the best performance directly followed by polynomial regression models. In this work, we use the following inputs:

$$P_r = \frac{p_2}{p_1}, T_r = \frac{T_{heater}[K]}{T_{w1}\ [K]}, p_{mean} = \sqrt{p_1 p_2}, \omega, T_1 \quad (1)$$

Standing for pressure ratio, temperature ratio, mean pressure, rotation speed, and inlet temperature respectively. Each target variable is modeled using a deep feedforward neural network implemented in TensorFlow/Keras with a consistent architecture: 5 input features, four hidden layers composed of 300–128–128–300 neurons respectively, ReLU activation, and dropout regularization (rate = 0.2) after each hidden layer to reduce overfitting. The optimizer used is Adam with a default learning rate, and the loss function is mean squared error. A batch size of 20 is used for

training, with 200 training epochs and an internal validation split of 0.2. All input and output data are normalized to the range [0.1, 0.9] to ensure training stability. The resulting mean absolute percentage error (MAPE) and R^2 score

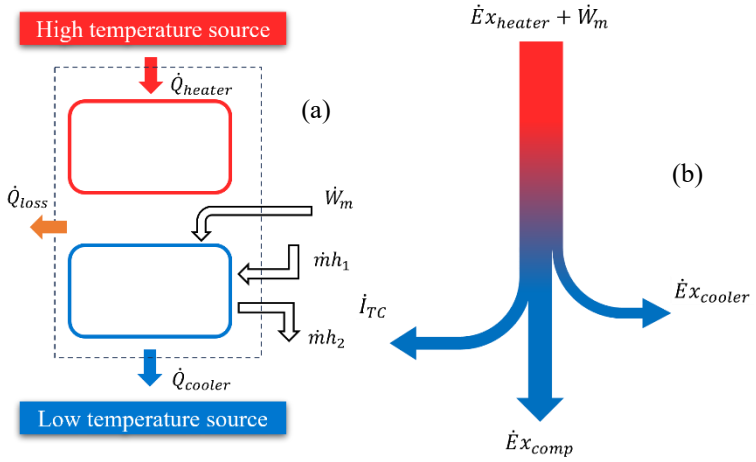

Fig. 3: (a) Energy and (b) Exergy flow diagrams of a TC.

of the model predictions are presented in Table 1. The resulting black-box models are considered reliable and suitable for exergy analysis at the system level. However, due to their black-box nature, they cannot be used to investigate exergy destruction sources within individual components. In fact, this is feasible with the detailed physical model derived in [3].

Table 1. Validation of ML models according to metrics MAPE and R2.

Parameters	MAPE (%)	R^2
$\dot{m}\ [\frac{kg}{s}]$	7	0.96
$T_2\ [K]$	5	0.94
$\dot{Q}_{heater}\ [W]$	6	0.95
$\dot{W}_m\ [W]$	6.9	0.92
$\dot{Q}_{cooler}\ [W]$	6.7	0.96
$\dot{Q}_{loss}\ [W]$	6	0.92

3 Exergy Analysis

3.1 Exergy Analysis of A TC

Whenever we have a temperature difference, useful energy can be recovered. The maximum useful energy or availability is what can be theoretically conceived by this temperature difference. This is where Carnot efficiency is put in use, in order to represent this energy potential. For TC, the exergy vectors seen in Fig. 3(b) are to be defined. Knowing that specific flow exergy is defined as:

$$\psi = h - T_0 s \tag{2}$$

T_0 being reference temperature. The rate of exergy transfer by heat into the TC (heater) can be represented as:

$$\dot{E}x_{heater} = \left(1 - \frac{T_0}{T_{heater}}\right)\dot{Q}_{heater} \tag{3}$$

The rate of exergy transfer to water on the cooler side (Fig. 2(a)):

$$\dot{E}x_{cooler} = \dot{m}_w(\psi_{w2} - \psi_{w1}) \tag{4}$$

To guarantee that energy balance is respected on TC, the heat recovered by the cooler is calculated as follows:

$$\dot{Q}_{cooler} = \dot{Q}_{heater} - \dot{Q}_{loss} + \dot{W}_m - \dot{m}(h_2 - h_1) \quad (5)$$

The rate of exergy transferred to the CO2 flow undergoing compression is:

$$\dot{E}x_{comp} = \dot{m}(\psi_2 - \psi_1) \quad (6)$$

Enthalpy and entropy are calculated knowing the temperature and pressure on the inlet and outlet sides using Coolprop [15]. The rate of exergy transfer by work is equivalent to the motor electric power $\dot{W}_m$. In steady state, the exergy balance can result in the following total exergy destroyed in a TC:

$$\dot{I}_{TC} = \dot{E}x_{heater} + \dot{W}_m - \dot{E}x_{comp} - \dot{E}x_{cooler} \quad (7)$$

Which contains the irreversibility resulting from flow and heat transfer (internal losses) as well as heat lost to the ambient (external loss). A more detailed analysis of how and where these irreversibilities occurr in a Stirling-type TC can be found in [12]. Exergy efficiency of a TC can thus be defined as follows:

$$\eta_{ex,TC} = \frac{\dot{E}x_{comp}}{\dot{E}x_{heater} + \max(\dot{W}_m, 0)} \quad (8)$$

Where max $(\dot{W}_m, 0)$ is used to avoid negative values since no mechanical work is actually recovered.

3.2 Exergy Destruction Analysis of A Ss-TCHP

The resulting exergy destroyed in a TC is to be compared with the other components in the ss-TCHP. The following assumptions are respected:

- The heat pump is considered in steady state regime.
- Pressure drops are neglected.
- Heat gains and losses are not considered.
- Potential and kinetic energy are not considered.
- Source of heat is considered to be waste heat, so combustion process and fume recovery are not considered.

We aim to find the exergy destroyed in each component and to show the exergy efficiency of a ss-TCHP when varying the main four inputs of a TC. p_1 and p_2 are considered known. The inlet temperature of the thermal compressor is set 3 K above the saturated vapor state, while the outlet temperature is predicted by the neural network model. The enthalpy at the outlet of the COND h_3 is considered at the saturate liquid state. The EEV is considered to be isenthalpic, so $h_3 = h_4$. Knowing that h_1 is calculated by eq. (5), the heat added to the EVAP and heat recovered by the COND are defined as follows, respectively :

$$\dot{Q}_{evap} = \dot{m}(h_1 - h_4) \quad (9)$$

$$\dot{Q}_{cond} = \dot{m}(h_2 - h_3) \quad (10)$$

The corresponding rate of exergies change of CO2 are defined as:

$$\dot{E}x_{evap} = \dot{m}(\psi_1 - \psi_4) \quad (11)$$

$$\dot{E}x_{cond} = \dot{m}(\psi_2 - \psi_3) \quad (12)$$

The exergy rate changes on the water sides are (Fig. 2(a)):

$$\dot{E}x_{w,evap} = \dot{m}_w(\psi_{w4} - \psi_{w1}) \quad (13)$$

$$\dot{E}x_{w,cond} = \dot{m}_w(\psi_{w3} - \psi_{w2}) \quad (14)$$

We adopted the exergy destruction formulations used in [6]. Since no work is recovered, the rate of exergy destroyed in an EEV is equivalent to the exergy potential:

$$\dot{I}_{eev} = \dot{m}(\psi_3 - \psi_4) \tag{15}$$

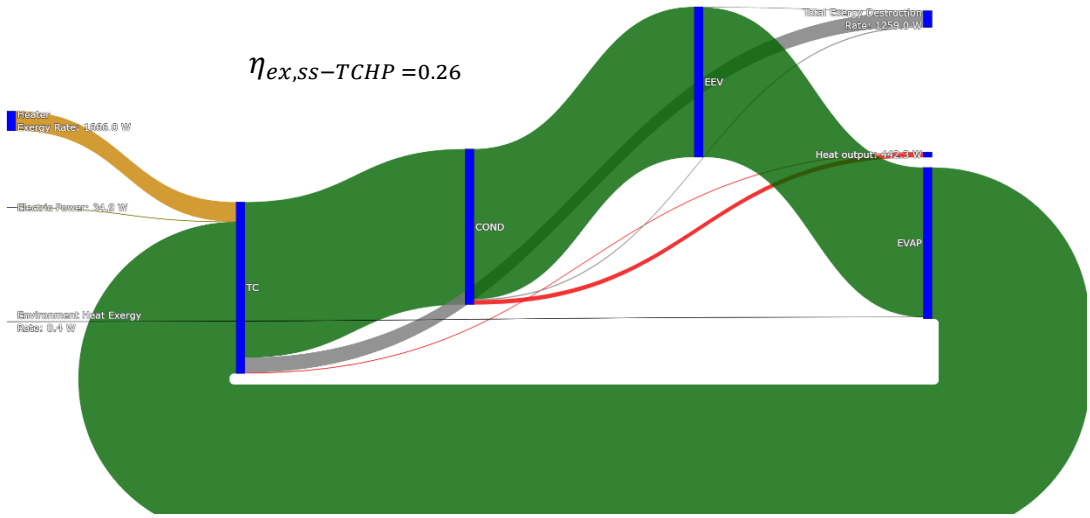

Fig. 4: Grassmann diagram showing the results of the exergy analysis on a ss-TCHP (Generated with plotly python library).

While the rate of exergy destroyed in EVAP and COND:

$$\dot{I}_{evap} = -\dot{E}x_{evap} + \dot{E}x_{w,evap} \tag{16}$$

$$\dot{I}_{cond} = \dot{E}x_{cond} - \dot{E}x_{w,cond} \tag{17}$$

The exergy flow and exergy destruction on a ss-TCHP are represented by the Grassman diagram (Fig. 4). Exergy efficiency of a ss-TCHP is defined as the exergy on the COND and cooler over the heater exergy:

$$\eta_{ex,ss-TCHP} = \frac{\dot{E}x_{w,cond} + \dot{E}x_{cooler}}{\dot{E}x_{heater} + \dot{W}_m} \tag{18}$$

4 Results And Discussions

In this section, a parametric analysis is carried out to show the influence of varying main inputs on the exergy destruction and exergy efficiency on TC and ss-TCHP. When varying one of the inputs, the other ones are kept constants: $P_r = 1.35$, $T_r = 3.32$, $\omega = 150\ rpm$, and $p_{mean} = 45\ bar$. The reference temperature and pressure are $T_0 = 273.15\ K$ and $p_0 = 1\ bar$. The ranges of the varying inputs are:

Table 2: Inputs ranges.

P_r	$\in [1.24, 1.63]$
p_{mean}	$\in [29, 55]$ bar
T_r	$\in [2.6, 3.69]$
ω	$\in [60, 260]$ rpm

The mean pressure, pressure ratio, rotation speed, and temperature ratio are varied to show their effects on the rate of exergy distribution in cooling and compression, as well as the variation of motor power. Fig. 5(a) shows an increase in compression exergy rate, a decrease in motor power, and a slight variation in the cooling exergy rate as the mean pressure increases. The exergy efficiency increases with mean pressure until it stabilizes at a maximum beyond 46 bar. Increasing the pressure ratio leads to an increase in motor exergy rates, as shown in Fig. 5(b). On the

other hand, the cooling exergy rate changes slightly, and the compression exergy rate increases until a pressure ratio of 1.33, after which it starts to decrease while the cooling exergy rate increases. The exergy efficiency is best when the pressure ratio is between 1.24 and 1.46, with a peak at 1.33. Increasing the motor rotation speed leads to an increase in the motor's electric power, along with a rise in compression exergy and a slight change in the cooling exergy rate. The exergy efficiency is best when the speed is between 100 and 190 rpm, with a maximum at 150 rpm, as shown in Fig. 5(c). A notable point to highlight is that at 60 rpm, the motor power becomes negative, which signifies that the TC runs solely on heat at that point. Fig. 5(d) shows that increasing the temperature ratio leads to a decrease in motor power, which is due to the increase in heater exergy compensating for the motor's electric power to maintain a speed of 150 rpm. The exergy efficiency is best between 2.6 and 3.3, with a maximum at 2.96. After 3.3, the cooler exergy rate increases and the compression exergy rate starts to decrease. Overall, Fig. 5 illustrates that the most significant factors affecting exergy efficiency are mean pressure and pressure ratio, while rotation speed and temperature ratio have a comparatively smaller impact.

To detect the thermodynamic inefficiencies according to components in an ss-TCHP, we extend the exergy analysis to include the EEV, EVAP, and COND, described by equations (15), (16), and (17), respectively, and the TC by equation (7). According to Fig. 6(a), as the mean pressure increases, the exergy destruction rate seems to increase in the heat exchangers and EEV, while it decreases in the TC, reaching a minimum at 46 bar. Exergy efficiency increases greatly as the high pressure increases. Since the pressure ratio is considered constant, an increase in mean pressure leads to a rise in high pressure and, consequently, in condensation temperature, while the inlet water temperature remains constant. As a result, heat transfer becomes more significant. Fig. 6(b) shows that when the pressure ratio is between 1.24 and 1.37, the exergy efficiency is at its best. The exergy destroyed in the TC slightly decreases, while it slightly increases in the EVAP, COND, and EEV. After 1.37, the trend reverses and the exergy efficiency decrease significantly. Increasing the rotation speed leads to a monotonic increase in exergy destroyed in the TC, while the increase in the other components saturates after 126 rpm. On the other hand, the exergy efficiency is highest between 100 and 193 rpm, with a maximum at 150 rpm (Fig. 6(c)). Fig. 6(d) shows that the exergy efficiency is best between 2.6 and 3.1, with a peak at 3. In this same range, the exergy destroyed in the TC slightly decreases, while it slightly increases in the other components. After a pressure ratio of 3.1, the exergy efficiency decreases exponentially: exergy destruction in the TC increases, while it decreases in the remaining components. Overall, Fig. 6 shows that the exergy destruction rate is by far the highest in TC, followed by the EEV, COND, and finally EVAP, where the exergy destruction rate is negligible. Mean pressure variation has the greatest impact on exergy efficiency, followed by pressure ratio, with smaller impacts from rotation speed and temperature ratio.

Both the TC and ss-TCHP exhibit similar variations in exergy efficiency with different inputs, which makes sense as the exergy destruction rate in the TC is by far the largest among all components, making it a primary target for optimization. A more detailed approach is needed to identify the sources of exergy destruction, which can be achieved using the detailed physical model developed in [3]. Additional data is required at higher operating pressures to investigate CO2 cycles in the transcritical regime, where such systems can offer higher efficiency in heating applications. The ranges of the other input parameters are already physically covered. Unfortunately, the current work is limited to the subcritical phase of CO2, unlike most studies in the literature that focus on transcritical operation. As a result, a direct comparison is not viable at this stage. The pressure ratio limitation of a single thermal compressor justifies the use of a multi-stage cycle, which enables CO2 to reach its transcritical state. This will be explored in future work by extending the exergy analysis to a three-stage TCHP configuration for a heating application, where transcritical operation is achieved and a more meaningful comparison can be made.

5 Conclusion

In this work, we introduced a Stirling-type thermal compressor technology integrated into a single-stage heat pump cycle. Performance and exergy analyses were conducted using TC data-driven models to evaluate variations in key input parameters: mean pressure, rotation speed, pressure ratio, and temperature ratio. An exergy analysis was performed on both the thermal compressor and the associated single-stage heat pump cycle. By assessing exergy destruction across various components, it became evident that the thermal compressor exhibited significantly higher exergy losses compared to other components. Consequently, optimizing the overall cycle requires a more detailed optimization of the thermal compressor, which should be examined through a more refined physical model. Future studies could explore alternative configurations of CO2 heat pump cycles utilizing thermal compressor technology to identify the most efficient design. Achieving the supercritical state of CO2 is highly encouraged in heat pump applications. Therefore, extending the mean pressure range could provide valuable insights into the performance of

thermal compressors at higher pressure levels and facilitate a comprehensive exergy analysis of a complete three-stage thermal compressor heat pump system.

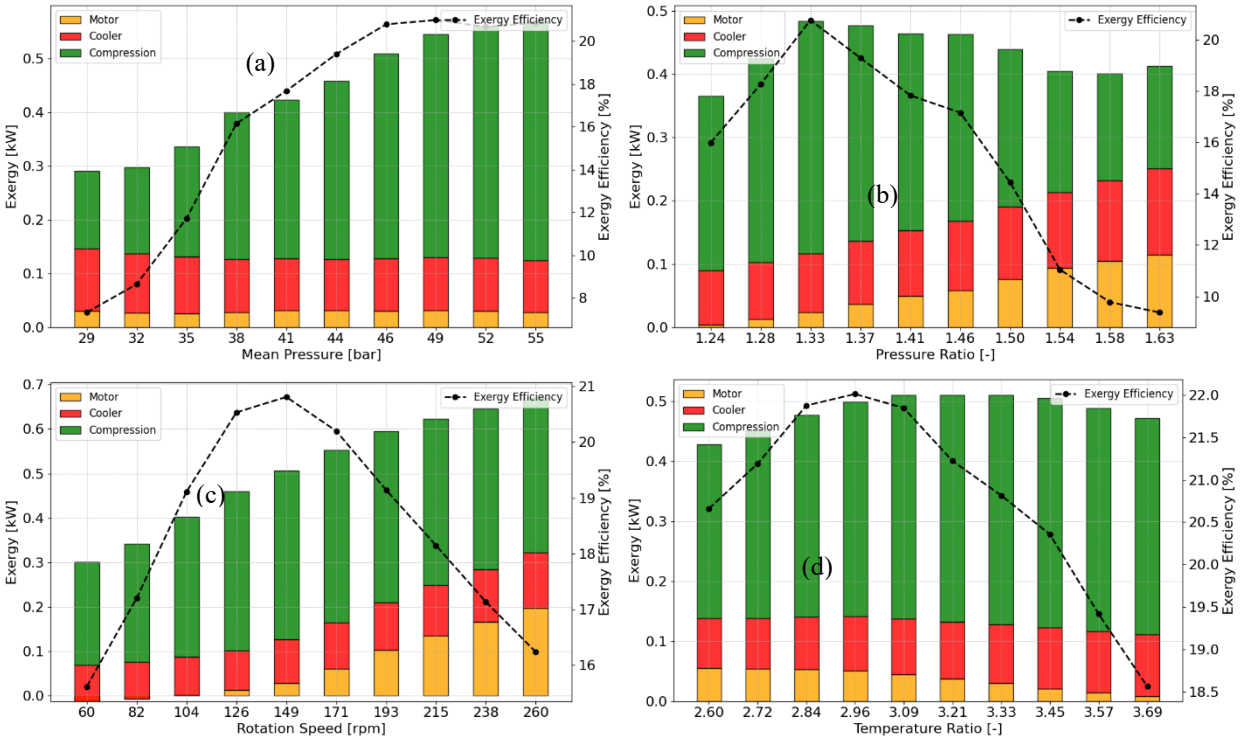

Fig. 5: Influence of (a) mean pressure, (b) pressure ratio, (c) rotation speed, and (d) temperature ratio on TC's exergy performance.

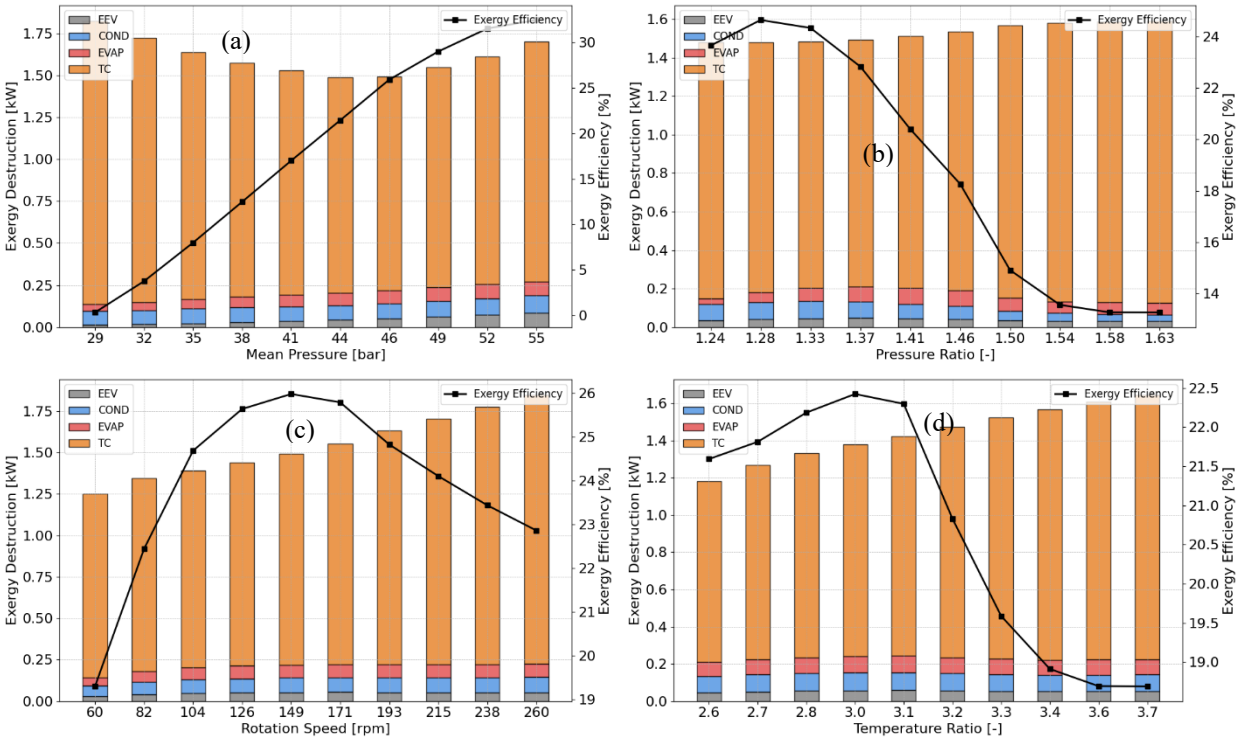

Fig. 6: Cycle exergy efficiency and exergy destruction according to components as a variation of (a) mean pressure, (b) pressure ratio, (c) rotation speed, and (d) temperature ratio.

Nomenclature

ψ	Specific flow exergy	(J/kg)
h	Specific flow enthalpy	(J/kg)
s	Specific flow entropy	(J/(kg.K))
p	Pressure	(Bar)
T	Temperature	(K)
P_r	Pressure ratio	(-)
T_r	Temperature ratio	(-)
ω	Rotation speed	(Rpm)
X_D	Displacer position	(m)
$\dot{m}$	Mass flow rate	(Kg/s)
$\dot{Q}$	Heat transfer rate	(W)
$\dot{E}x$	Exergy rate	(W)
$\dot{I}$	Exergy destroyed rate	(W)
η_{ex}	Exergy efficiency	(%)
$\dot{W}_m$	Motor power	(W)

Subscripts

COP	Coefficient of performance	(-)
MAPE	Mean absolute percentage error	(%)
CO2	Carbon dioxide	
EVAP	Evaporator	
COND	Condenser	
EEV	Electronic expansion valve	
TC	Thermal compressor	
Ss	Single stage	
TCHP	Thermal compressor heat pump	
Comp	Compression	
w	Water	
0	Reference	

References

1. Neksa, P., CO2 heat pump systems, Int J Refrig 25, p. 421–427, 2002.
2. Kühn, A., Thermally Driven Heat Pumps for Heating and Cooling, 2013.
3. Salame, A., Lemort, V., Dufour, P., Nadri, M., and Ibsaine, R., Dynamic Modelling Approach of a TC and Validation Based on Experimental Tests. ECOS24 conference proveedings, paper 193, 2024. https://ecos2024.com/proceedings/
4. Salame, A., Lemort, V., Dufour, P., and Nadri, M., An Empirical Model for a CO2 TC Based on Experimental Data. International Compressor Engineering Conference. Paper 2868, 2024.
5. Akau, R.L., Schoenhals, R.J., 1980. The second law efficiency of a heat pump system,Energy,Volume 5, Issues 8–9, Pages 853-863,ISSN 0360-5442.
6. Çengel, Yunus A., Boles, Michael A., Thermodynamics: an engineering approach. Boston: McGraw-Hill Higher Education, 2008.
7. Hofmann, M., Freißmann, J., Fritz, M., Alexe, J.H., Witte, F., Tsatsaronis, G., 2023. Exer-Based Methods For Heat Pumps. 7th International Seminar on ORC Power Systems, September 4 - 6, Seville, Spain, 2023.
8. Badescu, V., First and second law analysis of a solar assisted heat pump based heating system, Energy Conversion and Management, Volume 43, Issue 18, 2002, Pages 2539-2552, ISSN 0196-8904.
9. Yang, J.L., Ma, Y.T., Li, M.X., Guan, H.Q., Exergy analysis of transcritical carbon dioxide refrigeration cycle with an expander, Energy, Volume 30, Issue 7, 2005, Pages 1162-1175, ISSN 0360-5442.
10. J.A., Shilliday, S.A., Tassou, N., Shilliday, Comparative energy and exergy analysis of R744, R404A and R290 refrigeration cycles, *International Journal of Low-Carbon Technologies*, Volume 4, Issue 2, June 2009, Pages 104–111.
11. Ahamed, J.U., Saidur, R., Masjuki, H.H, 2011. A review on exergy analysis of vapor compression refrigeration system, Renewable and Sustainable Energy Reviews, Volume 15, Issue 3, Pages 1593-1600, ISSN 1364-0321.

12. Wang, J., Xi, X., Luo, K., Chen, L., Wang, J., Zhou, Y., Energy and exergy equilibrium analysis of Stirling-type TC (STC)—The core part in thermal-driven Vuilleumier machines, *Energy Conversion and Management*, Volume 199, 111961, 2019.
13. McGovern, J.A., Harte, S., An exergy method for compressor performance analysis, International Journal of Refrigeration, Volume 18, Issue 6, Pages 421-433, ISSN 0140-7007, https://doi.org/10.1016/0140-7007(95)98165-H, 1995.
14. Chollet, F., Keras. Github. Retrieved from https://github.com/fchollet/keras, 2015.
15. Bell, I.H., Wronski, J., Quoilin, S., Lemort, V., Pure and Pseudo-pure Fluid Thermophysical Property Evaluation and the Open-Source Thermophysical Property Library CoolProp, *Ind. Eng. Chem. Res.,* 53(6), p. 2498-2508, 2014.